**OMAE2017-62539**

# WAVE DRIFT FORCES AND LOW FREQUENCY DAMPING ON THE EXWAVE SEMI-SUBMERSIBLE

**Nuno Fonseca**
SINTEF Ocean
Trondheim, Norway
*nuno.fonseca @sintef.no*

**Carl Trygve Stansberg**
Ctstansberg Marinteknikk
Trondheim, Norway
*ctstansberg.marinteknikk @gmail.com*

## ABSTRACT

The paper presents realistic horizontal wave drift force coefficients and low frequency damping coefficients for the Exwave semi-submersible under severe seastates. The analysis includes conditions with collinear waves and current.

Model test data is used to identify the difference frequency wave exciting force coefficients based on a second order signal analysis technique. First, the slowly varying excitation is estimated from the relationship between the incoming wave and the low frequency motion using a linear oscillator. Then, the full quadratic transfer function (QTF) of the difference frequency wave exciting forces is defined from the relationship between the incoming waves and the second order force response. The process identifies also the linear low frequency damping.

The paper presents results from cases selected from the EXWAVE JIP test matrix. The empirical wave drift coefficients are compared to potential flow predictions and to coefficients from a semi-empirical formula. The results show that the potential flow predictions largely underestimate the wave drift forces, especially at the low frequency range where severe seastates have most of the energy.

## 1 INTRODUCTION

Diffraction codes based on potential flow theory tend to under predict wave drift forces on Semi-submersibles, especially in severe seastates (Stansberg 2001, Stansberg et al. 2015, Aksnes 2015). Conditions with waves and current in the same direction add complexity and increase discrepancies. The reason for the discrepancies appears to be viscous effects on the wave/structure interaction. Faltinsen (1990) discusses the horizontal component of normal drag forces on the pontoons, while the mean drag force on the columns above the still water level gives an additional contribution to the viscous drift force (Dev and Pinkster, 1994). Higher than second order potential flow effects may

also play a role. Both effects are neglected by second order potential flow methods. The consequence is that slow drift motions based on potential flow drift forces may be underestimated, as well as maximum mooring line tensions, compared to model test data, for example (Aksnes 2014, 2015).

One of the main objectives of the Exwave JIP is to improve today's procedures to calculate wave drift forces induced by severe seastates on floating structures, including current (Fonseca et al. 2016). The problem is tackled with a combination of dedicated model tests and numerical studies. Two structures are selected as case studies: a semi-submersible representative of a classical four column drilling rig and a FPSO hull. The present paper deals with the Semi, while another publication presents and discusses results for the FPSO (Fonseca and Stansberg, 2017). Fonseca et al. (2017) present a summary of the project results and progress until the end of 2016.

An important part of the work program consists of performing model tests, post-processing of the data and interpretation of results. The paper presents the Exwave Semi experimental program and the analysis performed to identify wave drift force coefficients from the test data. The procedure uses the irregular wave elevation and the low frequency measured motions time histories, together with a second order signal analysis technique, to identify the difference frequency wave exciting quadratic transfer function (QTF).

The empirical wave drift coefficients are compared with potential flow predictions, with predictions from a semi-empirical correction formula and with results derived from periodic wave tests. The potential flow results are computed by a diffraction code accounting for the wave-current interaction effects. The surge low frequency damping is estimated and discussed as well.

## 2 MODEL TESTS

Model tests were performed at the Ocean Basin Facility at MARINTEK during October 2015 with a 1:50 scaled model of the Exwave semi-submersible. This platform represents a classical drilling rig with four columns and two pontoons. Figure 1 shows a photo of the model, while Table 1 presents the platform main particulars.

The tests focused on the dynamic behaviour of the platform in waves and current. The aim of the model test program was to obtain test data to: (a) identify the slowly varying wave drift forces and the related slow drift damping and (b) assess the quality of slow drift motions numerical predictions. The focus is on the horizontal low frequency motions induced by severe seastates. The wave-current interaction effects on the wave drift forces are also addressed.



Figure 1: EXWAVE semi-submersible 1:50 scaled model.

Table 1: EXWAVE semi-submersible main properties.

| Parameter | Identification method | Unit | Model scale | Full scale |
|---|---|---|---|---|
| Length of pontoons | measured | [m] | 2.15 | 107.5 |
| Breadth outside pontoons | measured | [m] | 1.625 | 81.25 |
| Survival draft | observation of waterline | [m] | 0.46 | 23.0 |
| Displacement | weighted and obs. of wl. | [kg], [t] | 306 | 39206 |
| LCG | dry inclin. test & obs. of wl. | [m] | 0.0 | 0.0 |
| TCG | dry inclin. test & obs. of wl. | [m] | 0.0 | 0.0 |
| VCG | dry inclination test | [m] | 0.473 | 23.65 |
| GMT | inclination test in water | [m] | 0.047 | 2.36 |
| GML | inclination test in water | [m] | 0.050 | 2.48 |
| Rxx | Swing test | [m] | 0.721 | 36.1 |
| Ryy | Swing test & tuning num. model | [m] | 0.688 | 34.4 |
| Rzz | Assumed, not measured | [m] | 0.846 | 42.3 |

The tests were performed at 3 m water depth (150 m full scale), which may be considered as deep water conditions for most of the wave frequency range of interest.

The model was moored with a soft horizontal mooring system with (almost) linear restoring forces in surge and sway. The system is composed of 4 thin lines with horizontal angular separation of 45 degrees. Two lines attach at the model portside and two lines at the starboard side, with the other ends at the Ocean Basin sides. Each line includes a system of springs with designed stiffness. Decay tests identified the following surge natural periods:

- Uc = 0:         Tn = 116.5 s
- Uc = 0.97 m/s:  Tn = 115.2 s

Parameters such as the wave height and current velocity are changed systematically with the objective of characterizing their influence on the wave drift forces. Both regular and irregular wave conditions were used. System identification tests were performed as well.

The measured responses from the tests in waves include: wave elevation, vessel motions, accelerations at the deck, relative motions, global horizontal mooring system forces and mooring line forces at the fairleads.

The measured signals from the regular wave tests (periodic waves) are post-processed to identify their harmonic contents, namely the: mean value, 1st, 2nd and 3rd harmonic amplitudes and periods, and the response amplitude operator (RAO) and related relative phase angle. Some simple statistics are calculated as well.

The time records from the irregular wave tests are post-processed in terms of spectral analysis and statistical analysis. The analysis is carried out for: the signals as measured, low pass filtered signals and high pass filtered signals. The filtering frequency is 0.03 Hz full scale.

## 3 SECOND ORDER SIGNAL ANALYSIS

### 3.1 Theory

As described before in the text, potential flow numerical methods tend to under predict wave drift forces on floating structures, especially in severe seastates. The reasons might be viscous effects and higher than second order effects in the wave/structure interaction. Both are neglected by potential flow methods.

A method is followed in the present study to estimate realistic surge wave drift force coefficients for the EXWAVE semi-submersible. A post-processing analysis of the test data is carried out to extract empirical "wave drift coefficients" making use of a nonlinear data analysis known as "cross-bi-spectral analysis" to estimate characteristics of second-order (quadratic) responses (quadratic transfer functions – QTFs). Such drift coefficients might include higher-order contributions as well as purely quadratic contents. While a brief explanation is given in the following paragraphs, details of the method can be found in Stansberg (1997, 2001).

The procedure follows two major steps: first, identify the second order wave exciting force (or moment) signal from the measured motion responses; second, use the incident wave elevation and the estimated $2^{nd}$ order force, together with cross bi-spectral analysis, to identify wave drift force coefficients.

One assumes that the vessel motion in surge, sway or yaw, induced by irregular waves, may be represented by the following expansion:

$$x(t) = x^{(0)} + x^{(1)}(t) + x^{(2)}(t) + E_x(t) \qquad (1)$$

where $x^{(0)}$ represents a mean offset induced by the waves, $x^{(1)}(t)$ is the linear component of the motion, linear with respect to the linear component of the incident wave elevation, $x^{(2)}(t)$ is the second order motion component and $E_x(t)$ represent higher order effects.

Difference frequency effects dominate the horizontal second order motions and the sum frequency effects are not considered. A low pass filter is applied to $x(t)$ to remove the wave frequency response (and any higher harmonics). The

mean offset is removed as well, so that the resulting signal represents the slow drift oscillations $x^{(2)}(t)$.

The next step assumes the low frequency horizontal motions are decoupled, so that they may be represented by a one degree of freedom oscillator. The dynamic equation of motion is:

$$\ddot{x}(t) + 2\xi\omega_n\dot{x}(t) + \omega_n^2 x(t) = \frac{1}{m}g^{(2)}(t) \qquad (2)$$

where $\xi = c/2m\omega_n$, $c$ and $m$ are the system damping factor (or damping ratio), damping coefficient and mass, $\omega_n = 2\pi f_n$, $f_n$ is the natural frequency in Hz and $g^{(2)}$ is the 2nd order difference frequency wave exciting force. $\omega_n$ and $m$ are known from the model tests, while $\xi$ is estimated iteratively (further details ahead in the text), which allows an identification of $g^{(2)}(t)$.

The assumption of uncoupled low frequency horizontal motions is correct for head wave conditions, or beam waves and bow-aft symmetric vessels. For other headings, the assumption is usually accurate enough if the motions refer to a coordinate system with origin at the vessel centre of gravity.

An expansion similar to (1) represents the wave exciting forces:

$$g(t) = g^{(0)} + g^{(1)}(t) + g^{(2)}(t) + E_g(t) \qquad (3)$$

where $g^{(0)}$ is the mean wave drift force, $g^{(1)}(t)$ is the force response component linear with respect to the undisturbed incident wave elevation $\zeta(t)$ and it may be expressed as function of the complex Fourier transform of $\zeta(t)$ and of the complex linear force transfer function, namely $Z(f)$ and $H^{(1)}(f)$:

$$g^{(1)}(t) = \int_{-\infty}^{\infty}[Z(f)H^{(1)}(f)e^{i2\pi ft}]df \qquad (4)$$

One assumes the wave elevation follows a Gaussian distributed process with zero mean.

The second term of expansion (2), $g^{(2)}(t)$, represents the quadratic component, which can be represented by:

$$g^{(2)}(t) = \int_{-\infty}^{\infty}\int_{-\infty}^{\infty}[Z^*(f_m)Z(f_n)H^{(2)}(f_m,f_n)e^{i2\pi(f_m-f_n)t}]df_m df_n \qquad (5)$$

where $H^{(2)}(f_m,f_n)$ is the complex wave force quadratic transfer function (QTF).

The Fourier transform of $g^{(2)}(t)$ gives:

$$G^{(2)}(f) = \int_{-\infty}^{\infty}[g^{(2)}(t)e^{-i2\pi ft}]dt ,$$
$$f = (f_m - f_n) \qquad (6)$$

Cross bi-spectral analysis is applied to estimate the QTF. The cross bi-spectrum of $g^{(2)}(t)$ with respect to $\zeta(t)$ is given by:

$$S_{\zeta\zeta g}(f_m,f_n) = <Z^*(f_m)Z(f_n)G^{(2)}(f_m-f_n)> \qquad (7)$$

where $< >$ means statistical averaging.

Finally, manipulation of equations (5), (6) and (7) leads to an expression for estimation of the QTF (see Stansberg, 1997):

$$H^{(2)}(f_m,f_n) = S_{\zeta\zeta g}(f_m,f_n)/S_{\zeta\zeta}(f_m)S_{\zeta\zeta}(f_n) \qquad (8)$$

where $S_{\zeta\zeta}(f)$ is the wave spectrum.

Although the previous equations look simple, in practice achieving stable numerical solution for the QTF is not simple. The main difficulty is related to the statistical averaging in equation (7). Stansberg (1997) discusses further this aspect, where a particular noise reduction method is introduced based on imaging processing principles.

### 3.2 Example

This Section presents an example of results from the cross bi-spectral analysis for a long crested seastate with 2.5 m Hs and Tp nearly constant between 5 and 25 s (broadband wave spectrum). The semi-submersible heading is 0 degrees, which means the pontoons are aligned with the wave propagation direction and there is no current. The test duration was 3.3 hours, full scale, and the initial 20 minutes were removed before the time signals were used for the cross bi-spectral analysis.

Figure 1 shows the estimated surge QTF of the difference frequency wave exciting forces. The bi-frequency plane axes are in Hz and the colours represent the wave drift coefficients magnitude in kN/m$^2$. Dashed white lines follow diagonals with constant difference frequency of 0.0086 Hz, which corresponds to the surge natural frequency.
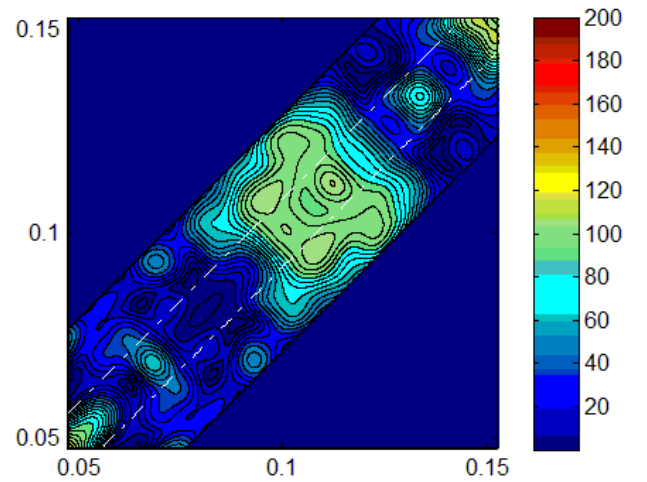


Figure 1: Empirical surge QTF: heading = 0 deg., Hs = 2.5 m, broadband wave spectrum, Uc = 0. Horizontal axes with frequency in Hz and drift coefficients in kN/m$^2$.

The quality of the identified QTF is assessed by comparing the measured low frequency motion with the same motion calculated using wave exciting forces reconstructed from the identified QTF (the latter is calculated solving equation 2). The comparison is done in terms of time histories and low frequency spectra. An example is presented in Figures 2 and 3 for the same seastate. The agreement between measured and reconstructed signals is good, which validates the QTF empirical estimation.
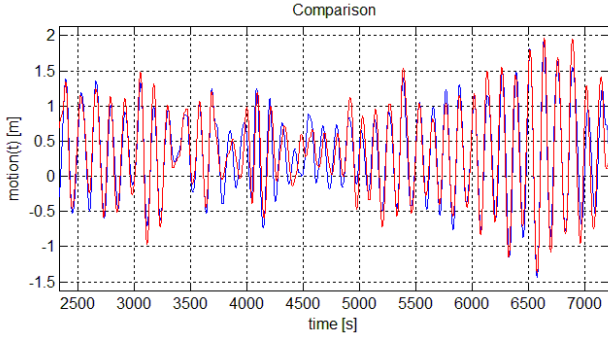
3

Figure 2: Comparison between measured slow drift surge motion (blue line) and reconstructed from the identified empirical QTF (red line).
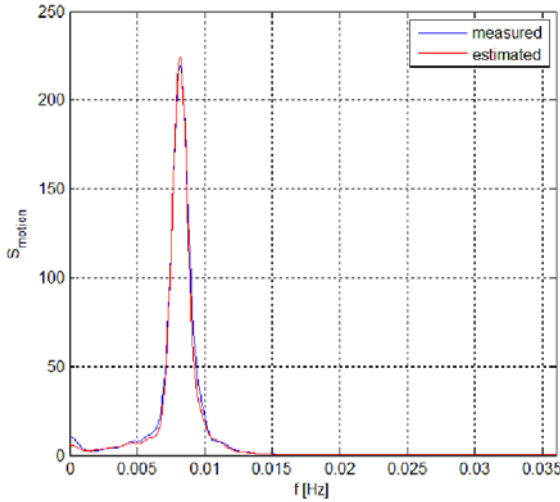


Figure 3: Spectra of low frequency surge motion. Comparison between experimental spectra (blue) and reconstructed spectra calculated from the identified QTF (red).

# 4  MEAN WAVE DRIFT FORCE COEFFICIENTS

## 4.1 Numerical model

Potential flow hydrodynamic coefficients, first order wave exciting forces and mean wave drift forces have been estimated by a 3D linear radiation-diffraction flat panel method (MULDIF, Hermundstad et al. 2016). The hull was modelled using 8956 panels, where the largest element diagonal is 2.3 m. Figure 4 presents the numerical model mesh.
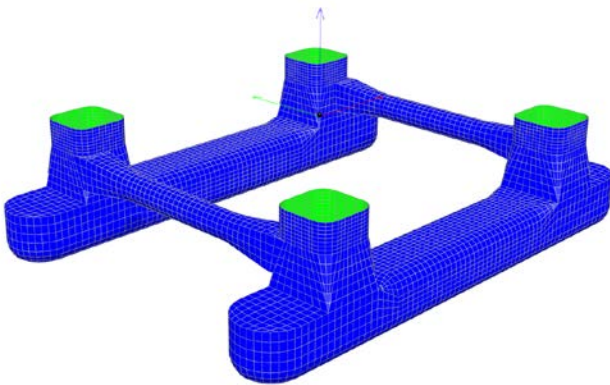


Figure 4: Hull mesh for MULDIF hydrodynamic calculations.

## 4.2 Semi-empirical correction formula

Stansberg at al. (2015) proposed a semi-empirical correction formula to estimate the wave drift force coefficients on column based semi-submersibles. The correction accounts for viscous effects and wave-current interaction effects and it was pointed as a short term alternative, while more advanced and commonly accepted procedures are not yet in place. Viscous drift forces are particularly important in large seastates and conditions with combined waves and current.

The surge/sway wave drift force coefficients in collinear waves with frequency $\omega$ and current ($U$) conditions is:

$$f_D(\omega, U, H_s) = f_D^{pot}(1 + C_p U) + B(GU + H_s) \qquad (9)$$

where the first term represents potential flow drift forces including a correction due to wave-current interaction and the second term represents the viscous drift component. Note that the last term including the significant wave height $Hs$ is a third order term; i.e. the resulting drift coefficients include a contribution that increases linearly with $Hs$.

Additionally:

- $f_D(\omega, U, H_s) = \frac{F_D(\omega, U, H_s)}{A^2}$ and $F_D$ is the mean wave drift force in harmonic waves with amplitude $A$.
- $f_D^{pot}$ is the mean wave drift force coefficients from 1st order potential flow theory with zero current.
- $C_p$ is a potential flow wave-current interaction coefficient, assumed as 0.25 s/m.
- $B = B' d_{sum}$, with $B' = kp$.
- $d_{sum} = \sum d_i$ is the sum of columns diameters.
- $k = 2\pi/\lambda$ is the wave number and $\lambda$ is the wavelength.
- $p = e^{-1.25(kD_0)^2} \ [kN/m^3]$ and $D_0$ is the main columns diameter.
- $G = 10 \ [s]$ represents a viscous wave-current factor determined empirically.

Stansberg at al. (2015) provide further explanations on the formula. The formula results will be referred in the following graphs as "MARINTEK-DNV/GL formula".

## 4.3 Wave drift force coefficients identified from irregular wave tests

The surge and sway mean wave drift force coefficients, corresponding to the zero difference ($\Delta f$) frequency components of the quadratic transfer functions (QTF), were extracted from the empirically estimated QTFs. In fact, an approximation is applied, instead of extracting directly the zero $\Delta f$ coefficients from the QTF. Since the slow drift motion spectra have more energy close to the natural frequency ($f_n$), the most relevant QTF estimates for actual motions are those at difference frequencies around $f_n$. The identification is assumed more accurate for the frequency range where response spectrum has more energy. For this reason, the procedure consists of extracting a diagonal with $\Delta f$ between $\Delta f = 0$ and $\Delta f = f_n$.

The approximation described above is valid if the QTF changes slowly around the main diagonal corresponding to $\Delta f = 0$ (which is the same as saying the QTF is nearly constant along diagonals with constant $f_1 + f_2$). The assumption is

similar, but not the same, to that of the Newman's approximation for the QTF off-diagonal terms (Newman, 1974). Figure 1 above with the empirical QTF shows that in fact the empirical drift coefficients for this semi change slowly around the main diagonal (the dashed lines represent diagonals with $\Delta f = f_n$).

The empirical coefficients are compared with potential flow predictions and with the MARINTEK-DNV/GL formula (see Section 4.2). The potential flow predictions were carried out with MULDIF for zero current velocity. The force coefficients, normalized by the wave amplitude squared, are given as function of the wave frequency.

Figure 5 shows the results for small, moderate and severe seastates. The low seastate is represented by a broadband spectrum with Hs = 2.5 m and the wave energy nearly constant between 5 and 25 s, while the moderate and severe cases correspond to Torsethaugen seastates. There is no current and the vessel heading is 0 degrees.

The low seastate graphs shows good agreement between the empirical wave drift coefficients and the potential flow predicted ones. Since the significant wave height for test is small (Hs = 2.5 m), it is expected that the potential flow results represent correctly the wave drift forces. The fact that the agreement is good indicates the cross bi-spectral analysis method is able to identify the wave drift coefficients.

One observes that the empirical coefficients increase with the significant wave height within the frequency range between 0.06 and 0.11 Hz. The potential flow coefficients are similar to the empirical ones for the small seastates, but they under predict the empirical ones for the moderate and large seastates. For the largest seastate, the difference between the potential flow and the empirical drift forces is very large at the low frequency range. One should note that most of the wave energy is concentrated in this low frequency range – the seastates peak frequencies are 0.062 and 0.080 Hz.

The current velocity increases significantly the wave drift forces for collinear wave and current conditions. The effect is illustrated in the graphs of Figure 6, which presents results for the largest seastate (Hs = 15 m and Tp = 16 s) and the three current velocities (Uc = 0, 0.82 and 1.58 m/s). The potential flow predictions, computed assuming Uc = 0, largely underestimate the identified wave drift force coefficients.

The semi-empirical formula results agree quite well with the empirical drift coefficients. However, the formula accuracy still needs to be checked for additional conditions, namely wave headings different from head waves and non-collinear wave and current, as well as for other semi-submersible geometries.
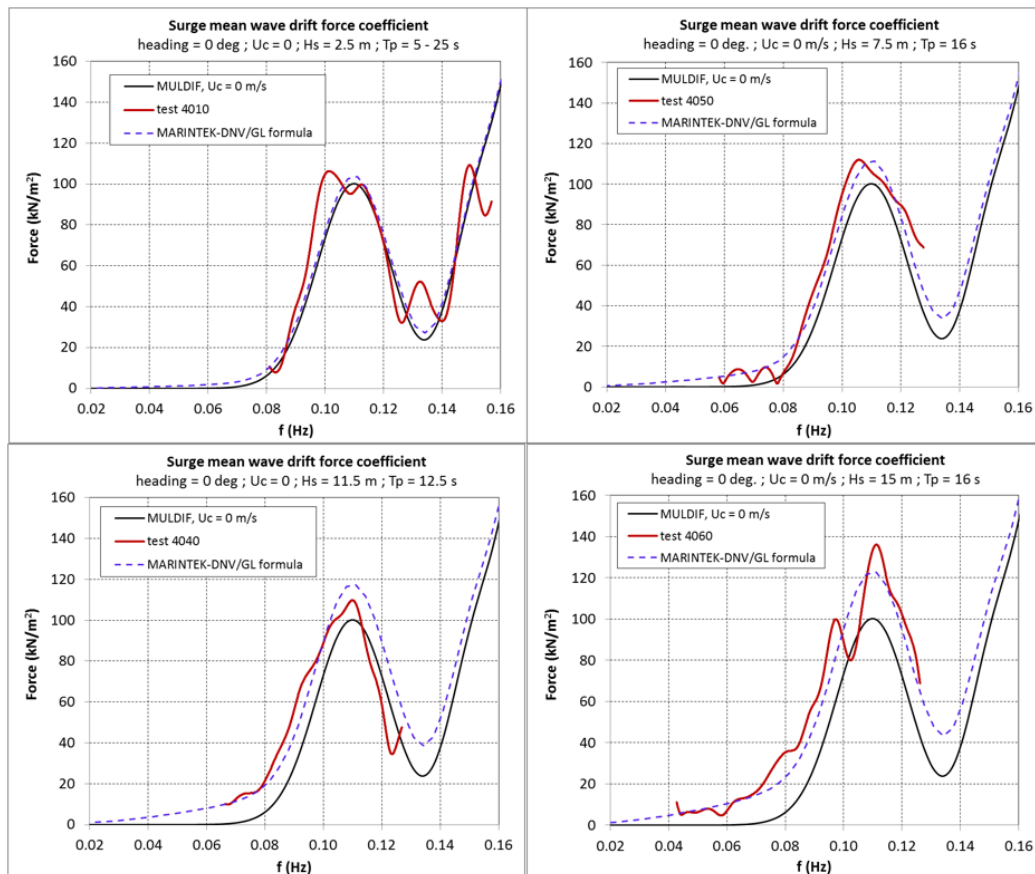


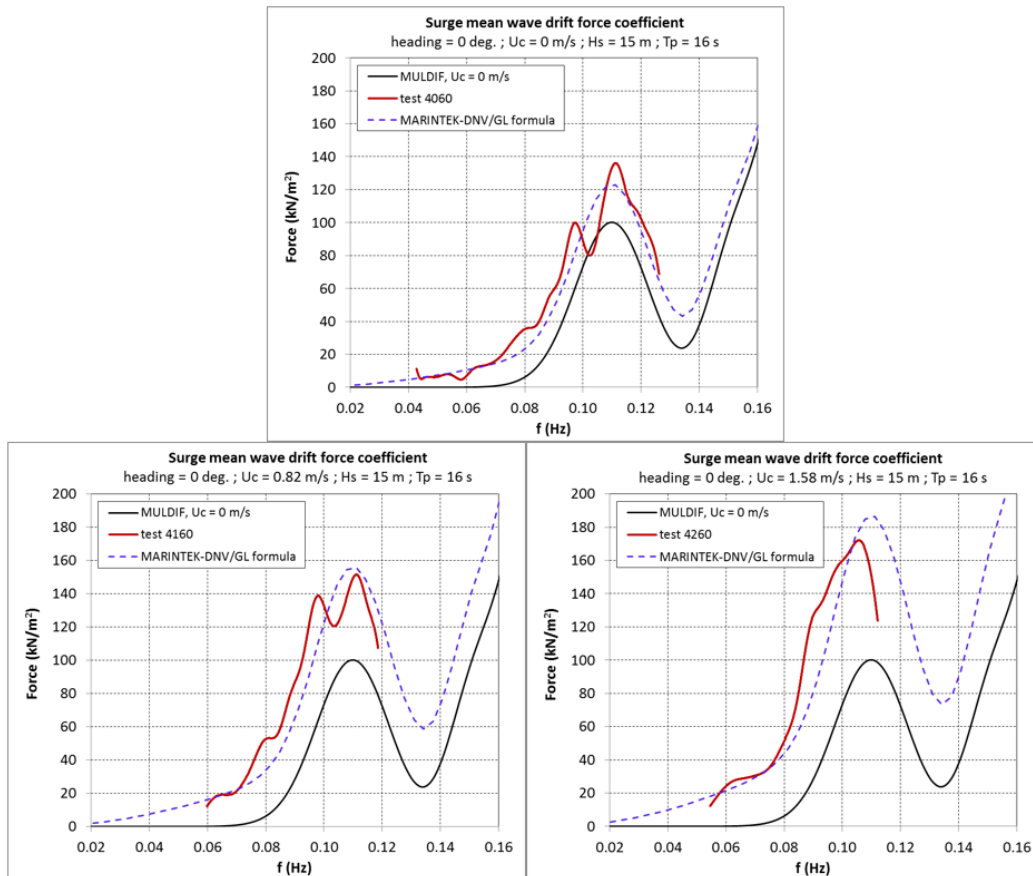Figure 5: Surge mean wave drift force coefficients: heading = 0 deg., 4 different seastates and Uc = 0.

Figure 6: Surge mean wave drift force coefficients: heading = 0 deg., Hs = 15 m, Tp = 16 s, Uc = 0, 0.82 and 1.58 m/s.

## 4.4 Wave drift force coefficients identified from periodic wave tests

This Section presents the mean wave drift force coefficients identified from the tests in periodic waves and compare them with the potential flow code predictions, coefficients identified from the tests in irregular waves and the predictions using the correction formula (see Section 4.2).

The wave drift force in harmonic waves is constant, therefore these forces are extracted from the measured mean horizontal total mooring system force. The method to identify the mean wave drift forces follows a few simple steps:

(a) The mean force with current only is identified from the initial 150 to 250 s of the force time traces, before the model encounters the first waves.

(b) Select the limits of the time record to identify the mean force, typically between 10 and 20 wave cycles after the transient vessel motion dies out.

(c) The difference between the mean force in waves and the mean force with current only defines the surge mean wave drift force.

(d) The results are presented as mean wave drift forces normalized by the incident wave amplitude squared (1st harmonic amplitude).

Figures 7 shows the surge mean wave drift force coefficients identified from the tests in periodic waves and 0 degrees heading, as function of the wave frequency (circle markers). The current velocity of 0.82 m/s is collinear with the waves.

The legend associated to each marker represents the incident wave 1st harmonic amplitude. The periodic wave results are presented together with results from the cross bi-spectral (CBS) analysis and the MULDIF predictions. The latter were calculated for Uc = 0 and 0.82 m/s.

The first observation is that the drift coefficients in periodic waves are qualitatively similar to the ones identified by the CBS analysis.

Furthermore, the coefficients identified in periodic waves are larger than the potential flow coefficients for low frequencies and the difference increases with the wave amplitude. This is an indication that the wave drift forces are "more than quadratic" with respect to the incident wave amplitude, which is probably related to a viscous drag contributing to the mean wave drift forces.

For the highest frequency, the periodic waves empirical drift coefficients are similar to the potential flow predictions, which seems to indicate that viscous drift is much less important for moderate and high frequencies. The results also show periodic wave results lower than those predicted from irregular wave tests. The reason for the discrepancies is still not clear.

Observation of MULDIF results with and without current shows that the linear potential flow wave-current interaction effects are very small for low frequencies. Wave-current potential flow codes are not able to represent correctly the capture the wave drift forces on semi-submersibles at the low frequency range, where severe seastates have most of the energy.
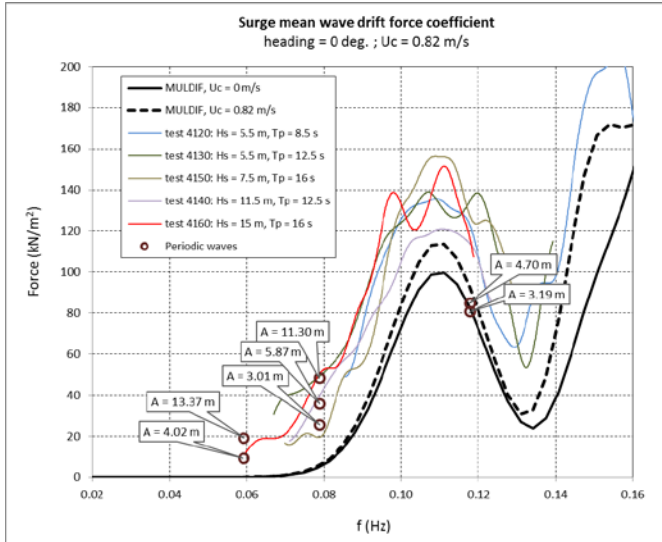
6

Figure 7: Surge mean wave drift coefficients in head waves and Uc = 0.82 m/s. Comparison between MULDIF results, coefficients identified from test data in irregular waves and from test data in periodic waves.

## 5 SLOW DRIFT DAMPING

As described in Section 3.2, the wave drift force coefficients estimation from irregular wave tests includes two major steps:
- First, the low frequency (LF) wave exciting force is estimated from the measured LF motion assuming the latter is represented by a linear mass-damper-spring system.
- Second, a cross bi-spectral analysis is applied to the wave elevation and the estimated response (excitation) to achieve the QTF.

Besides the excitation, the first step involves one additional unknown, namely the LF damping. For this reason, the QTF estimation follows an iterative process where the damping is systematically adjusted until a good convergence of the measured and reconstructed LF spectra is achieved. A linearized form of the LF damping is a result of the identification procedure. The present Section discusses these results.

The horizontal mooring linear stiffness is known a-priori and used to solve equation (2). Figure 8 shows the horizontal mooring restoring force identified from pull out tests. The stiffness is almost linear, with slight tendency for softening as the horizontal offset increases. One should note that most of the LF peaks, from all of the tests, have offsets lower than 40 m, therefore the mooring system may be considered linear in practice. The linear restoring coefficient for small displacements is:

$$K = 157 \ kN/m \qquad (10)$$

One additional piece of information useful for the present analysis if the linear and quadratic damping coefficients identified from the decay tests. Figure 9 presents the surge relative damping as function of the mean motion amplitude from a decay tests without current. It is possible to observe that the LF damping is nearly quadratic, with a small linear damping contribution. Table 2 shows system parameters

identified from the decay tests with Uc = 0 and 0.82 m/s, namely the surge natural periods, the linear damping coefficients ($B^L$) and the quadratic damping coefficients ($B^Q$). The surge total mass applied for the following analysis is:

$$m = 5.579E + 07 \ Kg \qquad (11)$$

where the zero current added mass was applied for conditions both with and without current.

The calm water linear and quadratic damping coefficients were applied to estimate an equivalent linearized damping, $B^*$. The surge low frequency damping forces by the linearized and by the quadratic models are given respectively by:

$$F_d^L = B^* \dot{x}_{LF}(t) \qquad (12)$$

$$F_d^Q = B^L \dot{x}_{LF}(t) + B^Q \dot{x}_{LF}(t)|\dot{x}_{LF}(t)| \qquad (13)$$

where $\dot{x}_{LF}(t)$ is the surge low frequency velocity.

Assuming the dissipation of energy, related to the damping forces, by the linearized and the quadratic models are the same, the linearized damping may be estimated as:

$$B^* = \frac{\int_0^T [B^L \dot{x}_{LF}(t) + B^Q \dot{x}_{LF}(t)|\dot{x}_{LF}(t)|] \dot{x}_{LF}(t) dt}{\int_0^T \dot{x}_{LF}(t) \dot{x}_{LF}(t) dt} \qquad (14)$$

where $\dot{x}_{LF}(t)$ is the surge low frequency velocity.
Equation (14) provides an estimation of the surge low frequency linearized damping in waves, if the linear and quadratic damping coefficients in calm water would remain unchanged for LF motions in waves. $B^*$ was estimated for several of the tested cases applying (14) together with the measured $\dot{x}_{LF}(t)$.
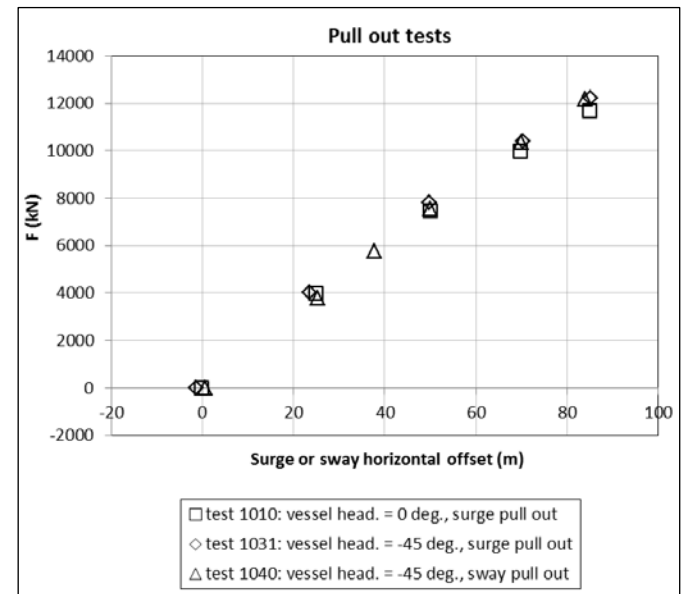


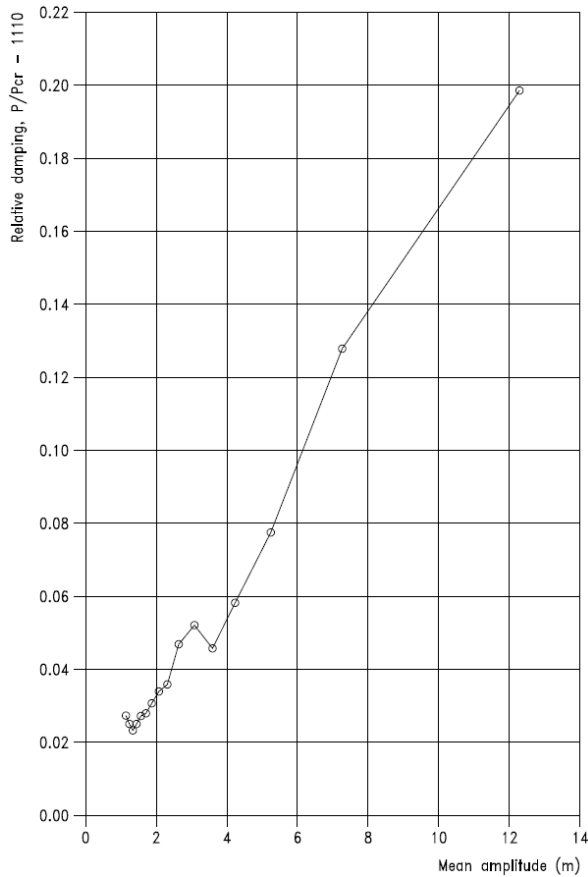Figure 8: Mooring system horizontal restoring force from pull out tests (K = 157 kN/m).

Figure 9: Surge relative damping (damp. factor) with Uc = 0

Table 2: Surge natural period estimated from the decay tests

| Mode | Uc [m/s] | Decay Tn [s] | $B^L$/m [1/s] | $B^Q$/m [1/m] |
|------|----------|--------------|------------|------------|
| Surge | 0.00 | 116.5 | 0.0025 | 0.0385 |
| Surge | 0.82 | 115.2 | 0.0174 | 0.0108 |

Table 3 presents the LF system parameters identified from the tests in waves for the test cases of Section 4.3:

- The first four columns include information on the tested conditions.
- Columns number five and six show the mean surge offset and the LF surge standard deviation in waves.
- Column number seven presents the surge natural period adjusted to achieve a good agreement between the measured and reconstructed LF surge spectra peaks.
- Column number eight includes the surge relative damping estimated from the cross bi-spectral (CBS) analysis procedure. This may be regarded as the actual linearized damping in waves.
- Column number nine presents the surge relative damping from formula (14). This is the linearized damping in case the damping coefficients in waves would be the same as identified from calm water tests.

The first comment relates to the surge natural period needed for good agreement of measured and reconstructed LF spectra: for the low seastate it is very similar to Tn identified from the decay tests, however it increases with the seastate severity. Tn increases 22 % for the largest seastate. There

appears to be an increase of the added mass with the seastate severity, however more detailed studies are needed to conclude.

Regarding the linearized damping of the actual LF motion (8th column), it is very small for the low seastate and it increases significantly for severe seastates, which would be expected since the damping is of quadratic nature and the LF amplitudes (and velocities) increase with the seastate (see the standard deviations).

The current velocity effect on the LF damping can be assessed by comparing three seastates with the same Hs and Tp (15 m; 16 s) and three currents. The damping increases significantly with the current velocity, up to a maximum of 46 % of the critical damping for the largest current.

It is interesting to note that, although the damping increases very much with the current velocity, the LF motion standard deviation still shows an increase. The reason is that the increase on the low frequency drift forces due to wave-current interaction dominates the damping increase. In fact, it is possible to observe in the graphs of Figure 6 that the drift force coefficients increase very much with the current velocity.

Table 3: Surge low frequency system parameters

| Head. (deg) | Uc (m/s) | Hs (m) | Tp (s) | Mean offset (m) | Stand. dev. (m) | Tn (s) | Rel. damp. CBS (%) | Rel. damp. decay coeffs. (%) |
|------|------|------|------|------|------|------|------|------|
| 0 | 0 | 2.5 | pink | -0.33 | 0.71 | 120 | 2.3 | 4.2 |
| 0 | 0 | 7.5 | 16.0 | -1.90 | 2.03 | 123 | 14 | 7.9 |
| 0 | 0 | 11.5 | 12.5 | -4.95 | 4.04 | 133 | 20 | 12.6 |
| 0 | 0 | 15.0 | 16.0 | -4.89 | 4.56 | 147 | 23.5 | 13.4 |
| 0 | 0.82 | 15.0 | 16.0 | -10.83 | 4.90 | 147 | 28 | 19.1 |
| 0 | 1.58 | 15.0 | 16.0 | -25.29 | 5.26 | 147 | 46 | - |

Figure 10 presents the damping factors of the two last columns of Table 3. The full circles represent the actual linearized damping in waves identified by the cross bi-spectral analysis procedure, while the open circles represent the damping estimated by equation (14). The latter is the damping that would be present if the linear and quadratic damping identified from the decay test would represent the damping in waves. The difference between the two sets of results represents the additional damping due to waves.

The first two points of Figure 10 (test 4010) correspond to the small seastate. One observes that the linearized damping estimated from the decay test coefficients is larger than the actual damping in waves. It is believed that the quadratic damping model from the decay test overestimates the damping for very small motion amplitudes and therefore it is not valid for the small seastate.

For the other seastes one observes an increase of the actual damping, compared to the predictions by the calm water damping model. The difference represents the damping increase due to wave effects – the damping in waves is larger than in calm water. The increase is partly related to modification of the wave drift forces due to low frequency surge velocity, also known as low frequency damping. One additional contribution may be related to additional viscous effects due to wave frequency relative motions between the vessel and the waves. The increase is between 60 and 80 % for the moderate and severe seastates without current and around 50 % for the case with current.
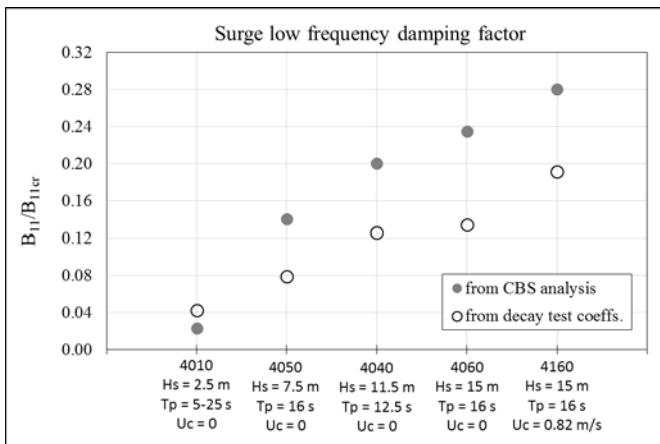
Figure 10: Surge low frequency damping factor

# 6 CONCLUSIONS

The paper presents and discusses horizontal wave drift force coefficients and low frequency damping coefficients for the Exwave semi-submersible under severe seastates. Model test data is used to identify the coefficients. A second order signal analysis technique is applied to identify the difference frequency wave exciting QTF.

Comparison of mean wave drift coefficients from different test cases shows the empirical drift coefficients increase with the seastate severity. Collinear wave-current interaction effects increase further the drift forces. Potential flow predictions largely underestimate the drift forces in severe sea conditions and in conditions with current, even if potential flow wave-current interaction effects are considered. The differences are especially notorious at the low frequency range where severe seastates have most of the energy. Results from periodic wave tests confirm the tendencies described in the previous paragraph.

A semi-empirical correction formula to calculate mean wave drift force coefficients in severe seastates with current shows quite good results as compared to the empirical coefficients. More detailed studies are needed to generalize this conclusion.

The surge low frequency damping increases significantly with the seastate severity and with the current velocity. Compared to the calm water damping, the damping in waves increases between 60 and 80 % for moderate and severe seastates without current and around 50 % for the checked severe seastate with current.

# 7 ACKNOWLEDGEMENTS

# 8 REFERENCES

Aksnes, V.Ø., 2014. "Correct" response in positioning analyses. Tekna Conference on DP and Mooring of Floating Structures Offshore, Trondheim, Norway, 12-13 Feb. 2014.

Aksnes, V.Ø, Berthelsen, P., Fonseca, N., and Reinholdtsen, S.-A., 2015. On the need for calibration of numerical models of large floating units against experimental data. Proceedings of the 25th International Ocean and Polar Engineering Conference, June 21-26, Kona, Hawaii, USA.

Dev, A.K. and Pinkster, J.A., 1994). Experimental evaluation of the viscous contribution to mean drift forces on vertical cylinders. Proc. 7th Int. Conf. on the Behaviour of Offshore Structures. (BOSS'94), Massach. Institute of Technology, Editor C. Chyssostomidis, Elsevier, Vol. 2, pp. 855 - 875.

Faltinsen, O., 1990. Sea Loads on Ships and Offshore Structures. Cambridge University Press.

Fonseca, N., Stansberg, C.T., Nestegård, Bøckmann, A., Baarholm, R., 2016. The EXWAVE JIP: Improved procedures to calculate slowly varying wave drift forces on floating units in extreme seas. Proc. of the ASME 2016 35th Int. Conf. on Ocean, Offshore and Arctic Eng., June 19-24, 2016, Busan, South Korea, paper OMAE2016-54829.

Fonseca, N. and Stansberg, C.T., 2017. Wave drift forces and low frequency damping on the Exwave FPSO. Proc. of the ASME 2017 36th Int. Conf. on Ocean, Offshore and Arctic Eng., June 25-30, 2017, Trondheim, Norway, paper OMAE2017-62540.

Fonseca, N., Ommani, B., Stansberg, C.T., Bøckmann, A., Birknes-Berg, J., Nestegård, A., de Hauteclocque, G., Baarholm, R., 2017. Wave Forces and Low Frequency Drift Motions in Extreme Seas: Benchmark Studies. Proceedings of the Offshore Technology Conference, paper OTC-27803-MS, 1-4 May 2017, Houston, TX, USA.

Hermundstad, E.M., Hoff, J.R., Stansberg, C.T. and Baarholm, 2016. Effects of wave-current interaction on floating bodies. Proc. of the ASME 2016 35th Int. Conf. on Ocean, Offshore and Arctic Eng., June 19-24, 2016, Busan, South Korea, paper OMAE2016-54868.

Newman N., 1974. Second-order, slowly-varying forces on vessels in irregular waves. Proc. Symp. on the Dynamics of Marine Vehicles and Structures in Waves, London, UK, 182-186, April 1974.

Stansberg, C.T., 1997. Linear and nonlinear system identification in model testing. International Conference on Nonlinear Aspects of Physical Model Tests, OTRC, Texas A&M University, College Station, Texas, 2-3 May 1997.

Stansberg, C.T. 2001. Data Interpretation and System Identification in Hydrodynamic Model Testing. Proc. of 11th Int. Offshore and Polar Eng. Conf., ISOPE, Stavanger, Norway.

Stansberg, C.T., Kaasen, K.E., Abrahamsen, B.C., Nestgård, A., Shao, Y., Larsen, K., 2015. Challenges in Wave Force Modelling for Mooring Design in High Seas. Proceedings of the Offshore Technology Conference, paper OTC-25944-MS, 4-7 May 2015, Houston, TX, USA.